sustainability

MDPI

Article

Sampling of Gas-Phase Intermediate Pyrolytic Species at Various Temperatures and Residence Times during Pyrolysis of Methane, Ethane, and Butane in a High-Temperature Flow Reactor

Zuhaib Ali Khan [1,*], Paul Hellier [1], Nicos Ladommatos [1] and Ahmad Almaleki [2]

[1] Department of Mechanical Engineering, University College London, Torrington Place, London WC1E 7JE, UK
[2] Carbon Management Technologies Institute, King Abdulaziz City for Science and Technology (KACST), P.O. Box 6086, Riyadh 11442, Saudi Arabia
* Correspondence: zuhaib.khan.17@ucl.ac.uk

Abstract: Air pollution in many major cities is endangering public health and is causing deterioration of the environment. Particulate emissions (PM) contribute to air pollution as they carry toxic polyaromatic hydrocarbons (PAHs) on their surface. Abatement of PM requires continuous strict emission regulation and, in parallel, the development of fuels with reduced formation of PM. Key processes in the formation of PM are the decomposition of hydrocarbon fuels and the synthesis of potential precursors that lead to the formation of benzene rings and thereafter growth to PAHs and eventually PM. Methane, ethane and butane are important components of natural gas and liquefied petroleum gas, and are also widely used in transportation, industrial processes and power generation. This paper reports on a quantitative investigation of the intermediate gaseous species present during pyrolysis of methane, ethane and butane in a laminar flow reactor. The investigation aimed to further the understanding of the decomposition process of these fuels and the subsequent formation of aromatic rings. The pyrolysis of methane, ethane and butane were carried out in a tube reactor under laminar flow conditions and within a temperature range of 869–1213 °C. The fuels were premixed in nitrogen carrier gas at a fixed carbon atom concentration of 10,000 ppm, and were pyrolysed under oxygen-free conditions. Intermediate gaseous species were collected from within the tube reactor at different residence times using a specially designed high-temperature ceramic sampling probe with arrangements to quench and freeze the reactions at entry to the probe. Identification and quantification of intermediate species were carried out using a gas chromatography-flame ionization detector (GC-FID). During methane pyrolysis, it was observed that as the concentration of acetylene increased, the concentration of benzene also increased, suggesting that the benzene ring is formed via the cyclo trimerisation of acetylene. With all three fuels, all intermediate species disappeared at higher temperatures and residence times, suggesting that those species converted into species higher than benzene, for example naphthalene. It was observed that increasing carbon chain length lowered the temperature at which fuel breakdown occurred and also affected the relative abundance of intermediate species.

Keywords: hydrocarbon fuel; pyrolysis; high-temperature sampling; PAH precursors; benzene ring; soot formation

Citation: Khan, Z.A.; Hellier, P.; Ladommatos, N.; Almaleki, A. Sampling of Gas-Phase Intermediate Pyrolytic Species at Various Temperatures and Residence Times during Pyrolysis of Methane, Ethane, and Butane in a High-Temperature Flow Reactor. *Sustainability* **2023**, *15*, 6183. https://doi.org/10.3390/su15076183

Academic Editor: Pallav Purohit

Received: 20 February 2023
Revised: 16 March 2023
Accepted: 27 March 2023
Published: 4 April 2023

1. Introduction

The environmentally adverse consequences of continued global reliance on fossil fuels are becoming increasingly apparent. These include the contribution of fossil-derived CO_2 to greenhouse gas emissions and climate change [1] and the reduction of local air quality and public health. Combustion pollutants including PAHs and soot are believed to be responsible for large numbers of premature deaths worldwide annually [2]. Given the

likelihood of reliance on combustion in transport [3,4] and other economic sectors for some time to come, there is a pressing need to develop fuels from renewable sources and to reduce the negative impacts on health of combustion-generated pollutants. Therefore, a greater understanding of the influence of fuel composition on the formation of harmful pollutants, such as PAH and soot, is necessary to ensure the sustainable use of these fuels, both with respect to decarbonisation and public health.

There is increasing research effort on developing renewable fuels from various organic feedstocks for use as single or blended fuels, in internal combustion (IC) engines and other combustion systems [5]. In considering the fundamentals of PAH and soot formation, the simplest of all fuel molecules are short-chain alkanes. There are several such molecules used currently as fuels, such as methane and ethane, which are constituents of natural gas, while methane is also the main constituent of biogas obtained from anaerobic digestion of organic matter. Methane has a high hydrogen-to-carbon ratio and is a preferred fuel in many applied combustion systems [6]. Ethane is the simplest alkane with a C-C bond and is sometimes considered a model molecule in the combustion of higher alkanes [7]. Butane is a key component of liquefied petroleum gas, present as both normal and branched isomers.

Methane, ethane and butane have been studied previously in various combustion systems, including flames [8–16], flow reactors [17–24] and combustion engines [25–27]. These studies reported that the molecular structure of hydrocarbon fuels plays an important role in the initial decomposition pathways at varying temperatures during combustion and pyrolysis. In a hydrocarbon molecule, the bond strength of hydrogen atoms attached to different carbon atoms varies significantly [28,29]. For example, in an alkane, the weakest hydrogen-carbon bond corresponds to a tertiary carbon atom, while the strongest corresponds to the primary carbon; the bond between a secondary carbon and hydrogen is the second weakest [30]. Therefore, the molecular structure of fuels is significant, as it affects the rate and position of the hydrogen abstraction process, with abstraction commencing earlier at the weakest available carbon-hydrogen (C-H) bond [30]. Methane has only a single carbon atom and its C-H bonds require a substantially higher temperature to break these strong C-H bonds [31]. Ethane has both C-H and C-C bonds, with the initial fuel breakdown commencing with hydrogen abstraction, resulting in unsaturated hydrocarbons (e.g., ethylene and acetylene) [32]. In the case of butane, primary and secondary C-H bonds are present, with the secondary bond breaking first, followed by the primary bonds. The availability of the secondary C-H bonds therefore increases average rates of hydrogen abstraction relative to ethane, where only primary bonds are present. Dandajeh et al. studied the effect of carbon chain length from C_1 to C_7 hydrocarbons on the formation of PAHs and soot. They found that increasing carbon chain length reduced the gas phase PAHs concentration at higher temperatures, while the opposite trend was observed with particulate phase PAHs, where concentration rose at higher temperatures [23].

Bunker et al. used Supersonic Expansion Molecular Beam sampling to identify reacting species during pyrolysis of hexane and benzene in a high-temperature flow reactor [33]. An in situ mass spectrometry technique was used to identify only gaseous species under supercritical conditions. A high concentration of biphenyl was reported, which formed via hydrogen abstraction from benzene and hexane fuels. During hexane pyrolysis, low concentrations of several other species were observed, ranging from C_5 to C_2 hydrocarbons which might have acted as precursors to biphenyl formation. Edwin et al. studied the thermal decomposition of hydrocarbons under subcritical pressure using a single-pass pyrolysis flow reactor and, as might be expected, they observed that high temperatures and residence times increased rates of thermal decomposition [33]. Unlike aromatic fuels, they found that branched hydrocarbons underwent the greatest amount of thermal decomposition. In addition, they found that a straight-chain alkane produced the maximum concentration of C_2 species. Dryer and Glassman investigated the gaseous species produced from the oxidation of CO and CH_4 using a water-cooled stainless steel sampling probe. The major species detected were carbon dioxide, water and carbon monoxide, while trace amounts of ethane, acetylene and ethanol were also detected [34].

Although previous research on C_1 to C_4 hydrocarbons has contributed to a better understanding of their pyrolysis and combustion, there persist gaps in the understanding of how their molecular structure impacts on the initial formation of PAHs and soot. There remains also a need to develop experimental methodologies that deliver further detailed insights into the decomposition of sustainable fuels from biomass [35] and the subsequent formation of PAH. The formation of benzene from short-chain alkanes has been reported in the literature by several researchers [8,36–42]. The study reported here complements previous studies through reporting for the first time the quantification of fuel decomposition products and intermediate species via a new methodology applied in a pyrolysis furnace facility used for the study of soot and PAH formation at combustion engine relevant conditions [43]. Although PAHs and soot formation from C_1 to C_4 hydrocarbons has been reported previously using the same pyrolysis furnace [24], this study extended the previous research by the addition of a novel high-temperature sampling probe which allowed identification and quantification of intermediate species during the formation of PAH precursors, PAHs and soot.

The aim of the research reported here is to elucidate further the effects of carbon chain length, temperature and residence time on the pyrolytic decomposition pathways of methane, ethene and butane that lead to benzene ring formation, PAH growth, and, eventually, soot. Experiments were conducted to detect the intermediate species during pyrolysis at various residence times by the accurate positioning of the sampling probe within the furnace tube and freezing reactions at the entry to the sampling probe through dilution with nitrogen. To the authors' knowledge, this is the first systemic investigation of these C_1 to C_4 hydrocarbon test fuels under pyrolytic conditions at a wide range of temperatures (869 °C to 1213 °C) and residence times (0.65 to 1.51 s) providing directly comparable results for the decomposition and formation of PAH precursors of each of the three hydrocarbons studied. The extended test methodology provided concentration measurements of additional intermediate species (for example C_3 and C_4), suggesting some additional pathways for the formation of the first aromatic ring. The novel high-temperature sampling method developed allowed for the collection of intermediate gaseous species at high temperatures by means of the use of ceramic materials for the sampling probe coupled with using air to cool the probe, and diluting the sample at the entrance of the sample tube with nitrogen so as to quench and freeze the reactions. In similar research reported in the literature, residence time is typically controlled by varying the reactants flow rate [44], while with the current design, the sample is taken at different depths of the reactor, thus ensuring that the disturbance to the flow conditions and temperature gradients are minimised. This study contributes to sustainability science by furthering the understanding of fuel composition effects on the emission of harmful pollutants from combustion, knowledge vital to the sustainable provision of clean and efficient energy for power and propulsion applications.

2. Experimental Methodology

2.1. Experimental Setup and Conditions

2.1.1. Sampling Generation

The pyrolysis of methane, ethane and butane were carried out in the absence of oxygen in a high-temperature tube reactor under laminar flow conditions and within a temperature range of 869–1213 °C. The external surface of the reactor tube was electrically heated to the desired temperature with the aid of a PID temperature controller. The tube had a length of 1440 mm and an inner diameter of 104 mm. The hydrocarbon test fuel was mixed homogeneously in nitrogen diluent preheated to 200 °C and the mixture entered the reactor at the bottom of the tube. The reactor temperature profile and its operation were described in detail previously [23,24,45–47]. The reactants were sampled along a length of the tube where the longitudinal temperature of the reactants was constant. For the study presented here, a novel sampling probe assembly was developed, with details of the probe shown in Figure 1. The probe allowed the collection of a small amount of gas sample along the axis

of the heated section of the reactor during fuel pyrolysis. Upon collection, the gas sample was immediately quenched by diluting it with nitrogen. Figure 1 shows the construction of the probe, which comprised two concentric ceramic tubes with inner diameters of 25 mm and 18 mm. Four stainless steel capillaries with a 3 mm internal diameter were used to extract the sample gas, supply nitrogen to dilute and quench the sampled gas, and also for conveying air to cool the ceramic probe walls.

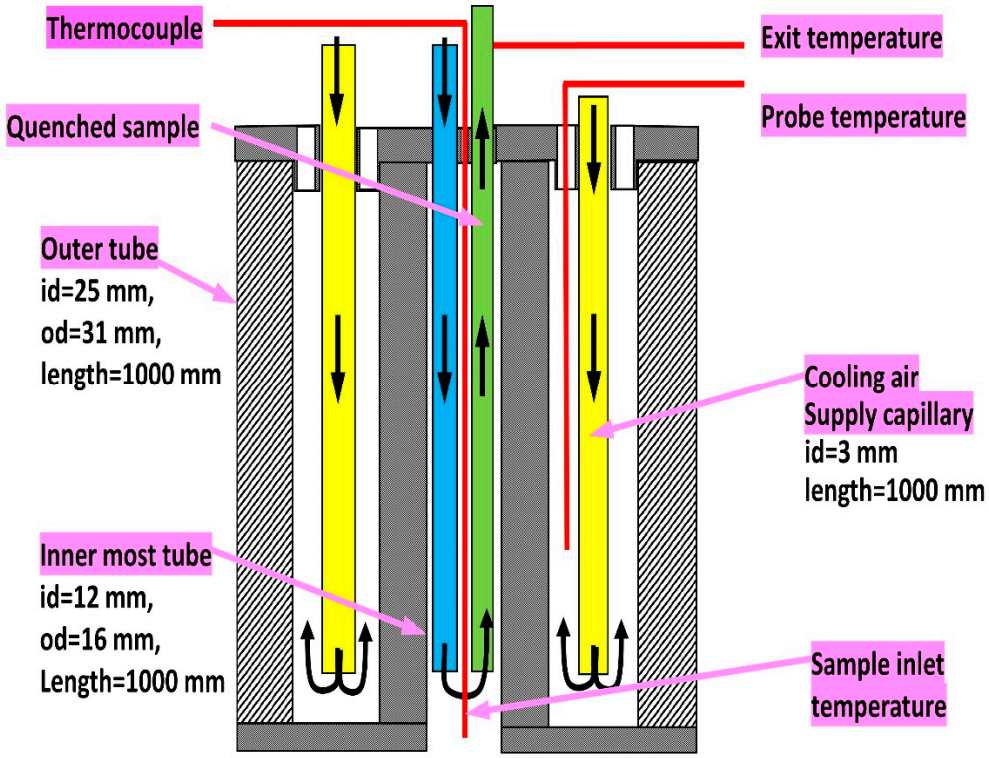

Figure 1. Schematic of the high-temperature reactor sampling probe.

The gas sample temperature was measured at entry to the sampling probe with a K-type thermocouple, with the measured temperature corrected for the heat gained through radiation from reactor tube walls. The reactor temperature control system controlled and displayed the temperature of the reactor tube wall. In order to control the gas sample real temperature accurately at the entrance to the sampling tube, a relationship was developed between the display temperature and the gas sample real temperature, which was corrected for radiative heat transfer. This relationship facilitated the setting of the controller temperature so that the desired sampling temperature was achieved accurately. All the sample gas inlet temperatures quoted in this paper are the real values corrected for radiative heat transfer.

The pyrolysis of methane, ethane and butane fuels was carried out at a fixed concentration of 10,000 ppm on a carbon atom basis in the heated nitrogen carrier stream flowing through the reactor tube and at gas sample inlet temperatures ranging from 869 to 1213 °C at atmospheric pressure. Oxygen-free nitrogen, metered through a mass flow controller, was used as the carrier gas with a fixed flow rate of 20 L/min (STP conditions).

2.1.2. Sample Collection

Figure 2 shows a schematic diagram of the tube reactor with its gaseous and liquid fuel supply lines (only gaseous fuels were used for this study). The figure also shows the system set up for gaseous species sampling. Figure 2 also shows thermocouples for monitoring and recording the sample temperatures at the inlet and exit from the sampling probe. The sampling probe was connected to a vacuum pump which drew out the mixture of gaseous sample and quenching nitrogen. Upstream of the vacuum pump, a 6 mm stainless steel tee

was installed with a septum for gaseous sample collection and injection into the GC-FID (see Figure 2). The flow rate of the sample and quenching nitrogen mixture was measured continuously by means of a rotameter and the rate was used to calculate the ratio of sample dilution with nitrogen from the known flow rate of quenching nitrogen measured with a metering mass flow rate controller.

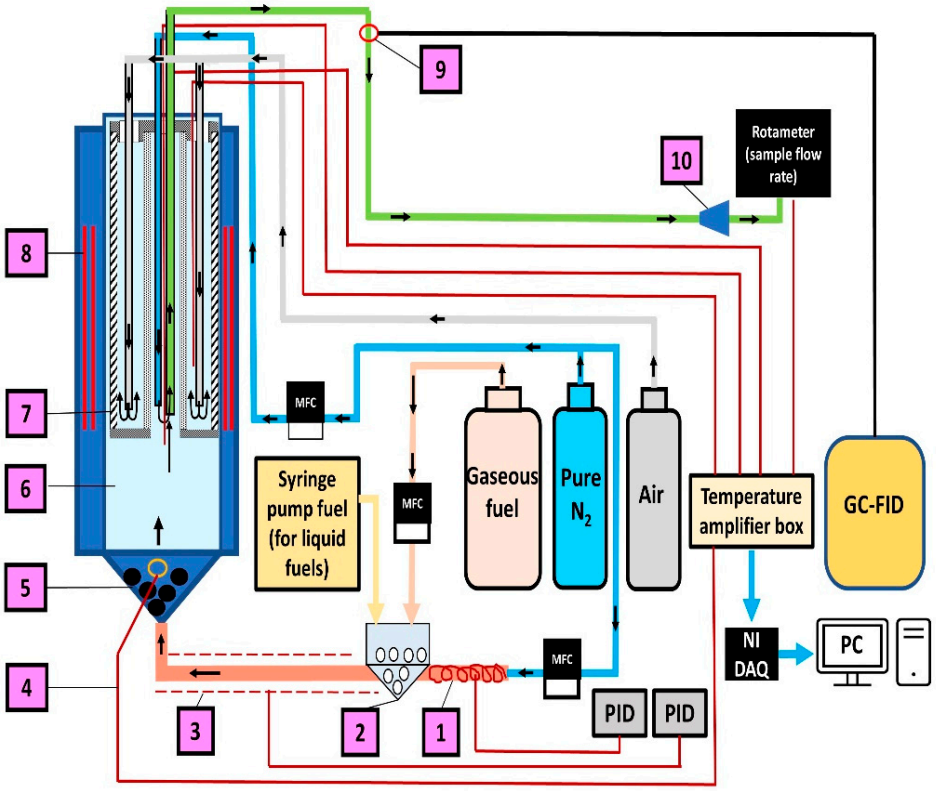

Figure 2. Schematic diagram of the tube reactor with gaseous and liquid fuel lines for gaseous species sampling. (1) N2 heater Fuel, (2) Vaporiser (liquid fuels), (3) Heated line, (4) Mixer temp, (5) N2/fuel Mixer, (6) Reactor tube, (7) Sampling probe, (8) Heating elements, (9) Sample extraction Septum for GC-FID, (10) Vacuum pump, PID: Temperature controller, MFC: Mass flow controller, NI DAQ: National Instrument data acquisition.

The sampling probe, which was used for the collection of intermediate fuel pyrolysis species, was inserted into the reactor and held at a specific depth which could be varied so as to control the residence time of the reactants. The gaseous reactants residence time was calculated using the tube reactor total gaseous volume flow rate at the measured real sample temperature, the cross-sectional area of the tube, and the depth of the sampling probe within the tube. Samples were collected at real sample gas temperatures (T) within the range of 869 °C to 1213 °C and at five different probe depths within the reactor tube: (81 cm, 76 cm, 71 cm, 66 cm, and 61 cm from the reactor top). For each reactor temperature (T), the residence times corresponding to these depths were calculated from the following relationships: 747/(T + 273) (s) (e.g., residence time of 0.65 s corresponding to depth of 81 cm at 869 °C); 1120/(T + 273) (s); 1493/(T + 273) (s); 1866/(T + 273) (s); and 2240/(T + 273) (s), respectively. This temperature range was selected for this study because preliminary experiments showed that the fuel molecules initiated decomposition and formed the final products (e.g., soot) within this temperature range. The selected residence times listed above were also informed by the preliminary experiments. These times was seen to encompass initial fuel decomposition, the formation of intermediate species smaller than benzene, and the formation of benzene. The K-type thermocouples used for measuring diluted quenched sample gas temperatures had ±2 °C uncertainty.

As mentioned above, in order to freeze the reactions immediately after the sample had been withdrawn from the reactor, a flow of nitrogen was used to quench and dilute the gas sample. Referring to Figure 1, the quenching nitrogen was supplied just inside the sampling probe tip and metered with a mass flow controller. The quenching nitrogen flow rate for reaction freezing was adjusted during the experiments to ensure that the sample exit temperature was always below 50 °C at location 9 in Figure 2. Gaseous samples were collected from the septum (see Figure 2) using a glass syringe. After collection, an internal standard (dichloroethane) was immediately added to the gas sample and the mixture was injected into the GC-FID shortly after the addition of the internal standard.

2.1.3. Gas Sample Analysis

The samples were analysed using GC-FID with an Agilent RT-Q-BOND (fused silica PLOT, 30 m × 320 µm × 10 µm) column. Pure helium was used as the carrier gas with a flowrate of 2 mL/min. A GC valve/immediate start was used with an injection volume of 1 µL in a split mode (2.5:1, 5 mL/min). The GC oven was heated initially to a temperature of 30 °C and then immediately ramped up with no hold period during the ramp as follows: to 40 °C at a rate of 5 °C/min; to 200 °C at a rate of 5 °C/min; and post-run at 200 °C for 1 min. The total run time for each sample was 34 min. The FID temperature was 250 °C and the flow rates of hydrogen, air, and makeup N_2 were 40, 400, and 20 mL/min, respectively.

For the identification of gaseous species using the GC-FID, an external standard mixture was used containing 11 selected species detailed in Figure 3. The selected species (up to C_6) were potential intermediates that contribute to the formation of benzene rings and PAHs growth. The species in the external standard mixture were at a 1000 ppm concentration diluted in nitrogen.

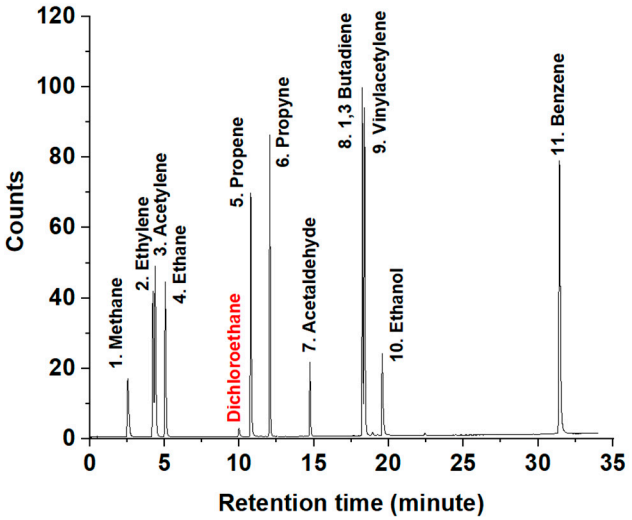

Figure 3. Sample GC-FID chromatogram of the 500 ppm external calibration standard with internal standard.

As the gaseous species produced during fuel pyrolysis can vary widely in concentrations, the external standard mixture of 11 species was serially diluted to create a further four concentrations of calibration standards (500 ppm, 300 ppm, 100 ppm and 25 ppm) using high purity nitrogen. The internal standard was dichloroethane (100 ppm) diluted in N_2. The internal standard was added to all the samples as well as to the calibration standards. For each of the 11 species in the calibration standards, a calibration curve was created by plotting the ratio of areas on the *x*-axis and the concentration ratio on the *y*-axis. For each of the resulting curves, a linear equation of best fit was generated. The regression coefficient R^2 was calculated for each of the linear calibration curves and all R^2 values were higher than 98%. Please note that two of the 11 species in the external standard mixture were oxygenates, that is ethanol and acetaldehyde, which were not expected to be present

during the pyrolysis of hydrocarbon fuels. These were included in the external standard because the same calibration mixture was also utilised for other projects taking place in the laboratory and involving oxygenated compounds.

2.2. Test Fuels

Three chemically high-purity alkane fuels (99.9%) were obtained from a specialist supplier of industrial gases (BOC). The properties for these alkane gaseous fuels (methane, ethane, butane) are shown in Table 1. These fuels were chosen because they allowed for the observation of effects on the formation of benzine (a PAH precursor), such as increasing carbon chain length and varying C:H ratio.

Table 1. Molecular structure and properties of selected alkane fuels [24,48,49].

Alkane Fuel	Molecular Structure	C:H Ratio	Molecular Mass (g/mole)	Boiling Point (°C)	Density (kg/m^3)
Methane	CH_4	0.25	16.04	−161.6	0.68
Ethane	C_2H_6	0.33	30.07	−88.6	1.28
Butane	C_4H_{10}	0.37	58.12	−0.5	2.48

During the experimental programme, the aim was to obtain the following observations and potential insights in the case of methane, ethane and butane:

- The initial temperature at which pyrolysis products were detected and the rate at which decomposition of the alkanes proceeded;
- The formation and conversion pathways of species contributing to benzene production;
- The influence of increasing carbon chain length on the quantities and distribution of potential PAH precursors.

3. Results and Discussion

In this section of the paper, experimental results will be presented, while the discussion of these results is left until Section 4, as this allows an overview of all the results to be maintained during the discussion.

3.1. Pyrolysis of Methane, Ethane, and Butane at a Constant Temperature of 869 °C

Figure 4 shows the concentration of species that were detected during ethane and butane pyrolysis at a constant temperature of 869 °C, and increasing residence time from 0.64 to 1.96 s. In Figure 4, and in subsequent figures, the error bars represent plus and minus one standard deviation from the mean value, where the mean value and standard deviation were obtained from three repeats at each residence time. Figure 4 shows the detected intermediate species only for ethane and butane fuels, with intermediate species for methane fuel not being shown in Figure 4. This is because at this relatively low temperature of 869 °C, no intermediate species were detected in the case of methane fuel, implying that pyrolysis of this fuel did not occur at any of the residence times considered.

It is interesting to note that at this temperature of 869 °C, C_3 and C_4 species were also detected along with C_1 and C_2 species in the case of butane fuels. Figure 4 also shows that as the residence time increased there was a general reduction in species concentration, with species larger than acetylene (C_2H_2) decreasing more rapidly.

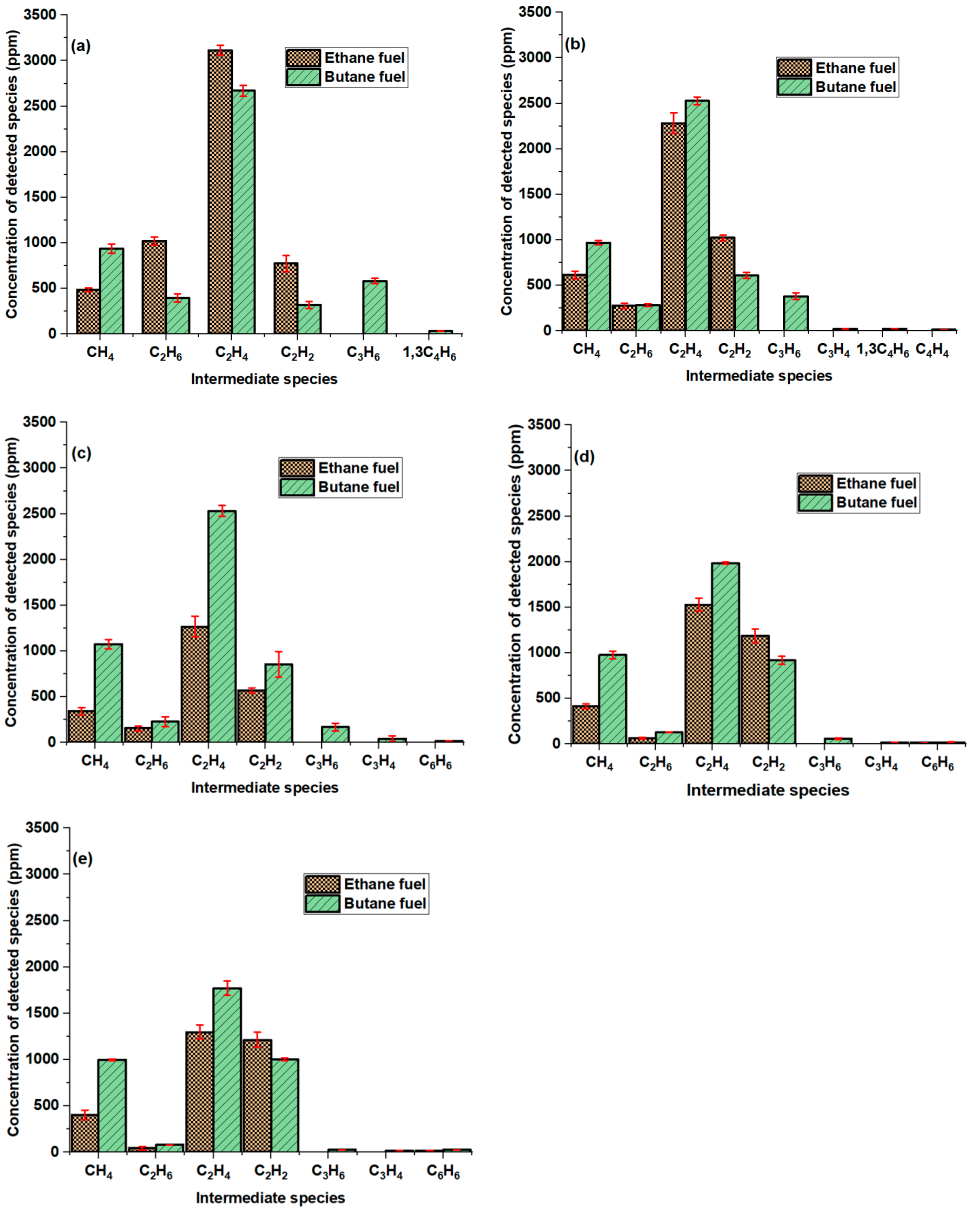

Figure 4. Concentration of detected species during ethane and butane pyrolysis at constant temperature of 869 °C and increasing residence time of (**a**) 0.65 s, (**b**) 0.98 s (**c**) 1.31 s, (**d**) 1.63 s, and (**e**) 1.96 s. Error bars denote one standard deviation. Note that no intermediate species were detected in the case of methane fuel at this temperature.

3.2. Pyrolysis of Methane, Ethane, and Butane at a Constant Temperature of 1018 °C

Figure 5 shows the concentration of species that were detected during ethane and butane pyrolysis at a higher constant temperature of 1018 °C, and increasing residence time from 0.58 to 1.74 s.

As in the case of the lower temperature of 869 °C (Figure 4), Figure 5 shows the detected intermediate species only for ethane and butane fuels, as apparently, pyrolysis of methane did not occur even at this somewhat higher temperature of 1018 °C. Figure 5 shows that the concentration of all detected species progressively reduced substantially as the residence time increased. In addition, only methane, ethylene and acetylene were detected in appreciable concentrations. Benzene was detected only at very small concentrations, and none was detectable at the longest residence time of 1.74 s.

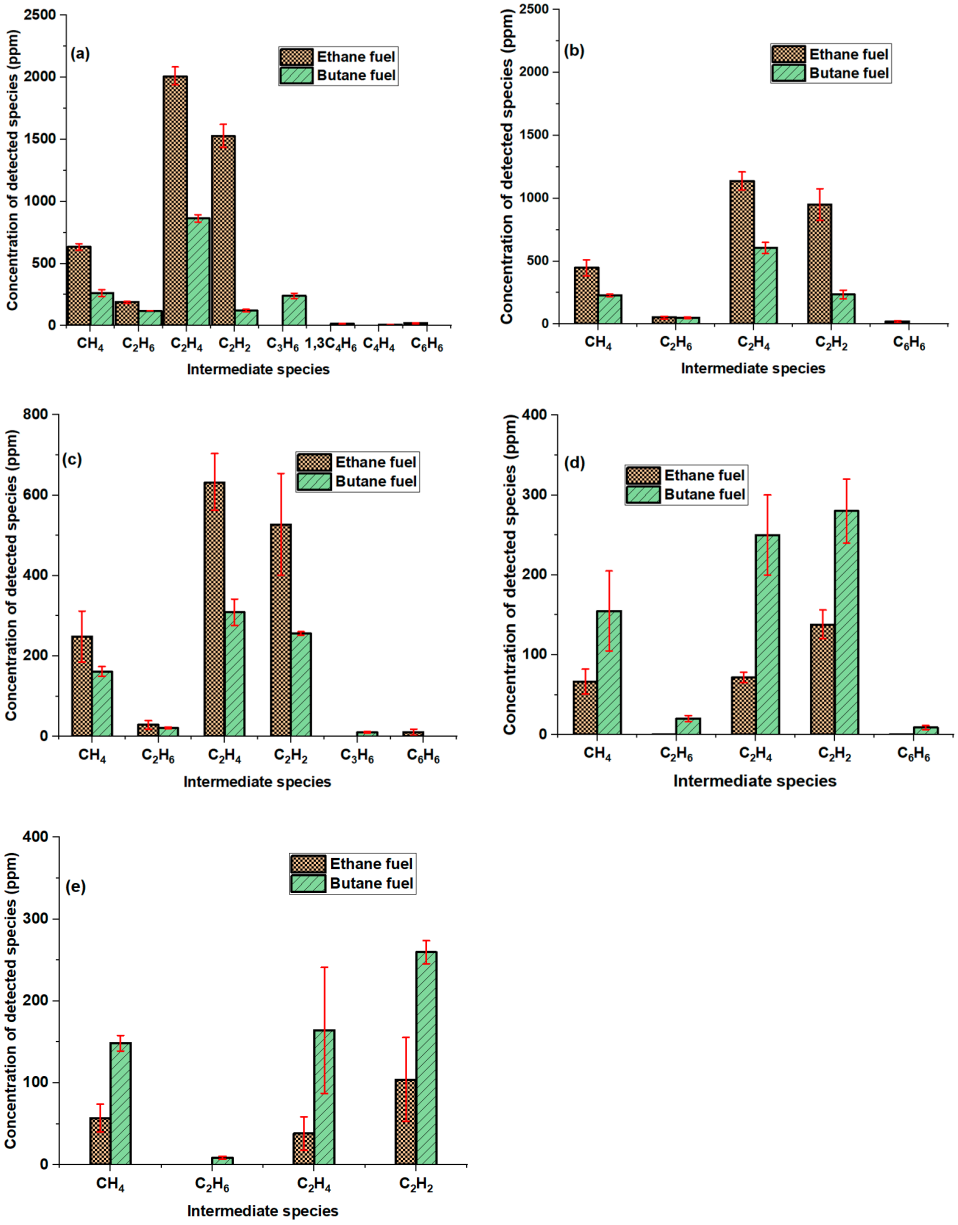

Figure 5. Concentration of detected species during ethane and butane pyrolysis at constant temperature of 1018 °C and increasing residence time of (**a**) 0.58 s, (**b**) 0.87 s, (**c**) 1.16 s, (**d**) 1.45s, and (**e**) 1.74 s. Error bars denote one standard deviation. Note: the *y*-axis is significantly magnified for (**c**–**e**). Note that no intermediate species were detected in the case of methane fuel at this temperature.

3.3. Pyrolysis of Methane, Ethane, and Butane at a Constant Temperature of 1120 °C

Figure 6 shows the concentration of species that were detected during methane, ethane and butane pyrolysis at a constant temperature of 1120 °C and increasing residence time from 0.54 to 1.61 s. At this higher temperature of 1120 °C, Figure 6 shows that pyrolysis of methane had now occurred, forming mainly C_2 species once the residence time increased beyond 0.54 s. Nevertheless, the pyrolysis rate of methane remained slow compared to that for ethane and butane, with 4900 ppm of methane still remaining at the longest residence time of 1.61 s.

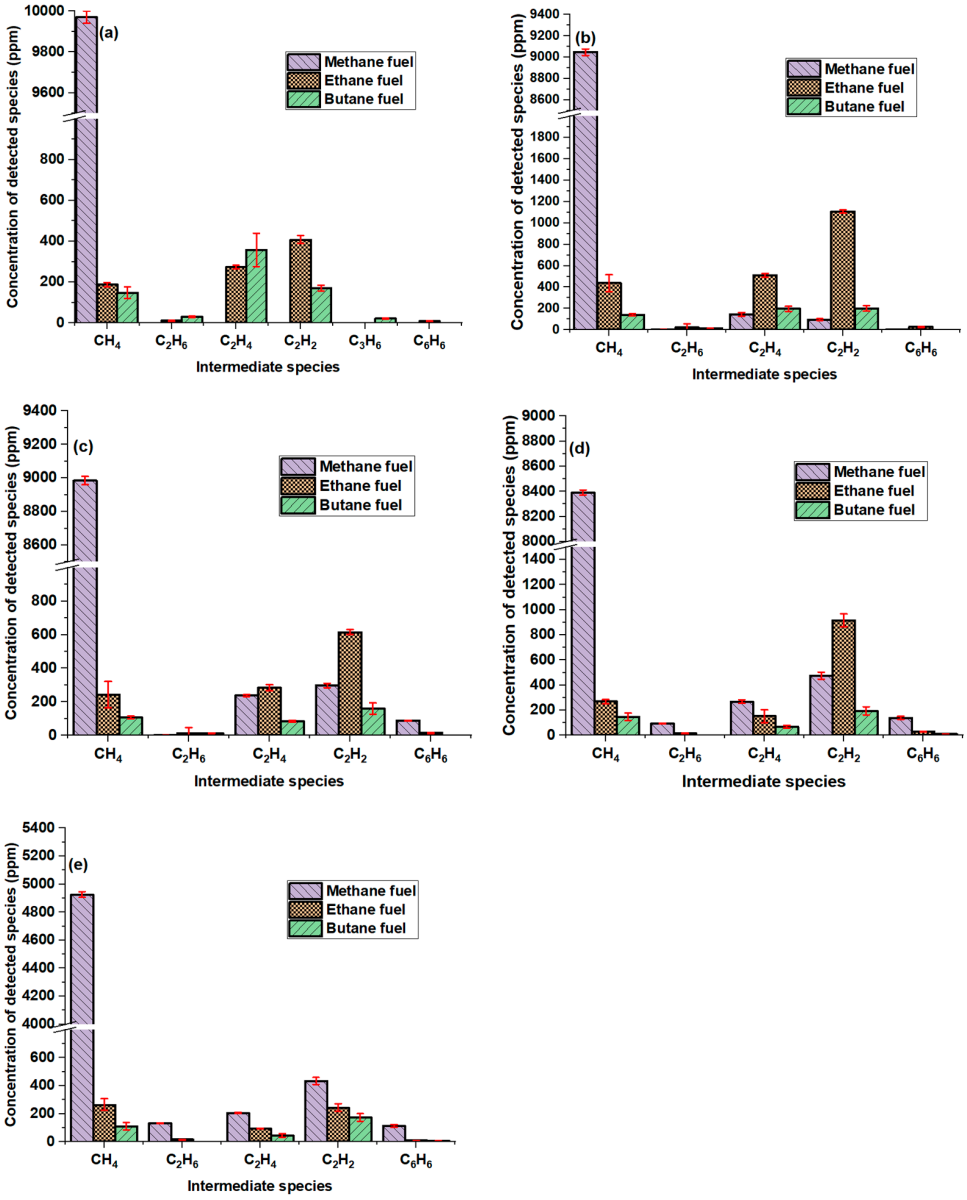

Figure 6. Concentration of detected species during methane, ethane and butane pyrolysis at constant temperature of 1120 °C and increasing residence time of (**a**) 0.54 s, (**b**) 0.80 s, (**c**) 1.07 s, (**d**) 1.34 s, and (**e**) 1.61 s. Error bars denote one standard deviation. Note: the *y*-axis value is significantly magnified in (**e**). Note the appearance of intermediate species from methane fuel at this higher temperature of 1120 °C.

3.4. Pyrolysis of Methane, Ethane, and Butane at a Constant Temperature of 1213 °C

Figure 7 shows the concentration of intermediate species that were detected during methane, ethane and butane pyrolysis at a constant temperature of 1213 °C and increasing residence time from 0.50 to 1.51 s. Figure 7 shows that the concentrations of all detected gaseous species decreased drastically relative to those at lower temperatures (Figures 4–6). This includes the intermediate species from methane fuel, which also now occur at substantial concentrations (see Figure 7), implying accelerated rates of pyrolytic reactions.

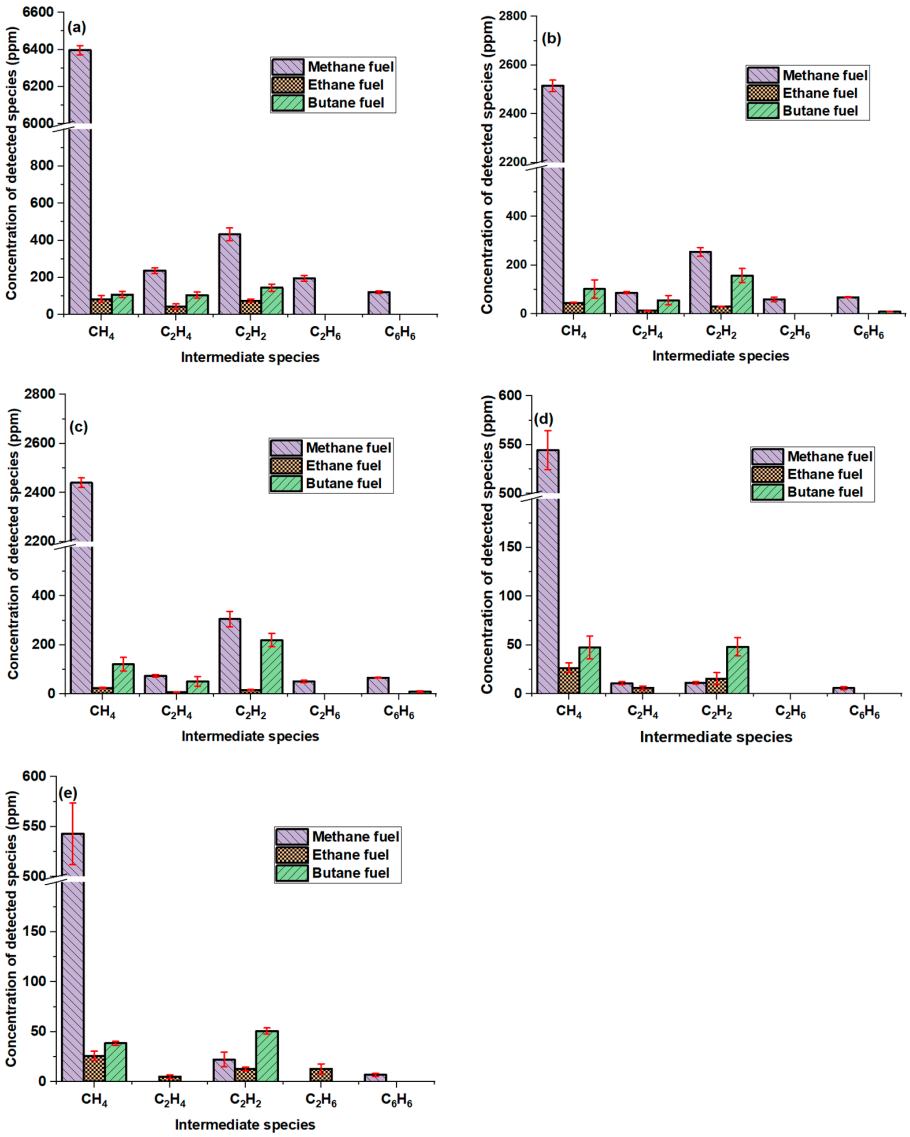

Figure 7. Concentration of detected species during methane, ethane and butane pyrolysis at constant temperature of 1213 °C and increasing residence time of (**a**) 0.50 s, (**b**) 0.75 s, (**c**) 1.00 s, (**d**) 1.26 s, and (**e**) 1.51 s. Error bars denote one standard deviation. Note: the *y*-axis is significantly less magnified in (**a**).

4. Discussion

4.1. Methane Fuel

This section discusses the results for methane fuel which was supplied to the reactor at a concentration of 10,000 ppmC in nitrogen. Gaseous samples were withdrawn from the reactor for analysis at sample probe inlet temperatures of 869 °C, 1018 °C, 1120 °C and 1213 °C, and a range of residence times (see Figures 4–7). It was found that at 869 °C and 1018 °C, almost all the supplied methane remained unreacted at all residence times considered; this was apparent from the detection of methane by means of GC-FID in the gaseous samples at approximately the supplied concentration (hence, data for methane fuel are not shown in Figures 4 and 5, corresponding to temperatures of 869 °C and 1018 °C, for the reasons explained here and previously). Therefore, for methane fuel, only results from temperatures above 1018 °C are discussed. Once the temperature was raised to 1120 °C, the concentration of methane in the sample reduced to approximately 5000 ppm at the longest residence time of 1.61 s (Figure 6e), indicating that significant methane pyrolysis was taking place. The pyrolysis rate increased further and substantially at the highest

temperature considered of 1213 °C and only 500 ppm of methane was detected in the sample extracted from the reactor at the longest residence time of 1.51 s (Figure 7e); that is, a tenfold reduction compared with the inflow methane concentration, when the reactor temperature was increased by 93 °C from 1120 °C to 1213 °C. Apparent from Figures 4–7 is that species other than unreacted methane were detected once the reactor temperature reached 1120 °C. These observations suggest that methane pyrolytic decomposition requires a temperature above 1018 °C and results in methane conversion to gaseous species including ethylene, acetylene, ethane and benzene. This observation is in agreement with thermodynamic studies of methane pyrolysis reported in the literature [31].

Figure 6a shows that at the shortest residence time of 0.54 s and a temperature of 1120 °C, none of the ten intermediate species investigated were found, with the methane fuel remaining the only compound detected at a concentration of 9800 ppm, which is close to the methane fuel inflow concentration of 10,000 ppm, suggesting that fuel breakdown had not yet started. As residence time increased, it is apparent from Figure 6 that the concentration of intermediate species present was initially dominated by ethylene and acetylene, with the addition of ethane appearing when residence times were increased to 1.34 s (Figure 6d) and then 1.61 s (Figure 6). This suggests that as residence times increased, ethane was initially a readily available and reasonably simple source of free radicals (H^-), hastening the consumption of methane fuel [49]. Once residence times became longer (>1.34 s) additional pyrolytic decomposition of methane took place, increasing the formation of methyl radicals and thereby the formation of ethane. As reported in the literature [49], the decomposition of methane is initiated by the loss of a hydrogen atom from the molecule to form methyl radicals, which subsequently combine to form ethane. It will be seen in a later section of this discussion that at higher reactor temperatures, ethane was present in the sample at considerably shorter residence times, suggesting that sufficient energy was available at higher temperatures to generate an abundance of free radicals from methane. Returning to Figure 6, at 1120 °C it can be seen that the ratio of ethylene to acetylene diminished with increasing residence time, suggesting dehydrogenation of ethylene to acetylene. For example, at the shorter residence time of 0.80 s (Figure 6b) more ethylene was present than acetylene, but as the residence time increased to 1.34 s (Figure 6d), the level of acetylene exceeded that of ethylene, with the concentration of acetylene becoming almost twice that of ethylene. It is interesting to note that as the concentration of acetylene increased, so did the concentration of benzene, suggestive of equilibrium. This apparent correlation between acetylene and benzene might also support the hypothesis that the formation of benzene from methane is via the cyclo-trimerisation of acetylene, as reported in the literature [50].

Figure 7 shows that at the highest tested temperature of 1213 °C, the pyrolytic breakdown of methane commenced at the shortest residence time of 0.50 s. It can be seen from Figure 7a that at this shortest time of 0.50 s, the concentrations of the intermediate species detected were at their highest levels. As the residence time increased, Figure 7 shows that the concentration of all species except acetylene decreased. This suggests the possibility that at longer residence times, these species converted into benzene rings and larger PAH species, and finally soot. Conversely, at short residence times, intermediate species concentrations are seen to be highest (Figure 7), suggesting that conversion of these species to benzene, PAHs and soot had yet to take place—especially at lower temperatures (Figures 5 and 6).

Figure 7 shows that at the highest temperature of 1213 °C and long residence times of 1.26 and 1.51 s, the acetylene concentration is at its lowest and there is an absence of any C_3 or C_4 species. These observations suggest that acetylene plays a role in the formation of benzene and in PAHs growth, mainly via the HACA mechanism. They also suggest that at this highest temperature, ethylene C-H bonds may have cleaved and formed triple-bonded acetylene, as ethylene was not detected at this high temperature and long residence times.

In conclusion, initiation of methane decomposition via pyrolysis required a reactor temperature greater than 1018 °C. The major gaseous species detected during methane

pyrolysis were C_2 (ethane, ethylene and acetylene) and C_6 (benzene), while C_3 and C_4 hydrocarbon species were not detected. Temperature and residence time had a considerable impact on the initial decomposition of methane, for example, on the relative abundance of C_2 species, and it is suggested that the formation of benzene is via acetylene through the cyclo-trimerisation of acetylene. The disappearance of the investigated species at higher temperature and longer residence times could be attributed to the faster formation rates of benzene and the growth of PAHs, as reported in the literature [24].

4.2. Ethane Fuel

This section discusses the results for ethane fuel supplied to the reactor at a concentration of 10,000 ppmC in nitrogen. Results are shown in Figures 4–7, which display the detected species at sample probe inlet temperatures of 869 °C, 1018 °C, 1120 °C and 1213 °C, and a range of residence times. Figure 4 shows that at the lowest temperature of 869 °C, the main products of ethane pyrolysis in order of decreasing concentration were ethylene and acetylene followed by methane, with very little benzene detected at any of the residence times considered. The presence of methane suggests an initial breakdown of the ethane fuel C-C bond to form methyl radicals, followed by hydrogenation to form methane [51]. It is also interesting to note that the level of methane remained approximately constant at all residence times at this low temperature of 869 °C. This observation suggests that once methane was formed, there was an absence of subsequent methane dehydrogenation; this suggestion is supported by an observation made above for methane pyrolysis (Section 4.1), where no conversion of methane was observed until 1120 °C.

Looking across Figures 4–7, it can be observed that there was a strong tendency for ethylene to be considerably more abundant at the two lowest temperatures of 869 and 1018 °C, and especially at shorter residence times, suggesting that ethane dehydrogenation is a dominant pathway to ethylene formation at these two lower temperatures.

Figure 4, corresponding to the lowest temperature of 869 °C, shows that there was a strong tendency for the concentration of acetylene to increase with increased residence time, while no benzene was detected, suggesting that any benzene formed quickly converted into higher PAH species via the addition of acetylene, for example through the HACA mechanism.

Figure 5, corresponding to the temperature of 1018 °C, shows that methane, ethane, ethylene and acetylene were all present at the shorter residence time of 0.5 s, which implies that the activation energy for a range of decomposition reactions had been reached at this temperature. The abundance of intermediate species at the shortest residence time and their relative scarcity at the longer residence times sampled, suggests a significant sensitivity of fuel decomposition and chemical kinetics to residence time at this temperature of 1018 °C.

It is interesting to note from Figure 4 that at the temperature of 869 °C, the concentration of ethylene was substantially greater than that of acetylene (more than twice as high at long and intermediate residence times), while Figure 5 shows that at the higher temperature of 1018 °C, there was greater parity, with the concentrations of the two species being considerably closer, suggesting a shift in the equilibrium between the two species. For example, at the temperature of 869 °C and a residence time of 1.31 s (Figure 4c) the concentration of ethylene was approximately two times that of acetylene, while at the higher temperature of 1018 °C and similar residence time the reverse was true, with the concentration of ethylene falling to 0.5 that of acetylene. The observation of higher levels of ethylene dehydrogenation to form acetylene with increasing residence time implies that at lower residence times, this reaction is rate limited, given that before 1.44 s there is a near complete absence of ethane (Figure 5d) from which ethylene was produced. Generally, it can be seen from Figure 5 that at the longest residence times of 1.44 s (Figure 5d) and 1.74 s (Figure 5e), the concentrations of intermediate species formed from the pyrolysis of ethane reduced significantly, suggesting their conversion to benzene and larger species, with the larger species being outside the detectable GC-FID range used and the scope of this study.

It is interesting to note that, as with methane pyrolysis, C_3 and C_4 species were not detected during ethane pyrolysis.

Figure 6 shows that at a pyrolysis temperature of 1120 °C the major products detected were acetylene followed by ethylene and methane. It can be observed from Figure 6 that substantial concentrations of acetylene were detected at all residence times, while at these residence times the concentration of ethane was barely detectable, possible due to its early rapid conversion to ethylene and other species. A more detailed examination of Figure 6 shows that at 0.80 s (Figure 6b), levels of methane, ethylene and acetylene all exceeded those at the earlier residence time of 0.54 s (Figure 6a), suggesting their formation from species other than ethane, given the very near absence of ethane at both these residence times. For example, an interesting possibility might be that acetylene was being formed not only via dehydrogenation of ethylene but also via the breakdown of species heavier than C_6 molecules (benzene), which would have been higher than the detectable GC-FID range used.

Figure 7 shows that at the highest temperature of 1213 °C and all residence times, all the intermediate species were found at only very low concentrations, suggesting rapid conversion to species heavier than benzene, including PAHs and soot (plus hydrogen).

It is apparent from Figures 4a, 5a, 6a and 7a (short residence times) that as the reactor temperature rises, the concentrations of ethylene tend to decrease, while those of acetylene increase. This observation suggests that the dehydrogenation of ethylene to acetylene becomes the primary reaction (note also the absence of substantial concentrations of ethane at higher temperatures). This observation suggests that the following reaction sequence reported in the literature [32] was prevailing during ethane pyrolysis:

$$C_2H_6 \rightarrow C_2H_4 \rightarrow C_2H_2$$

In conclusion, the decomposition pathways of ethane were affected by both temperature and residence time. Lower temperature and shorter residence times favoured the formation and accumulation of acetylene while higher temperatures and longer residence times favoured faster reaction rates and formation of species heavier than C_6 (benzene) not detectable within the GC-FID range considered (e.g., PAHs and soot). Ethane pyrolysis formed a significant amount of acetylene, which implies that the pathway for benzene formation and subsequent PAH growth could be via hydrogen abstraction and acetylene addition (HACA mechanism). Results show a relatively high abundance of the intermediate C_1 and C_2 species, with virtually no C_3, and C_4 species detected.

4.3. Butane Fuel

This section discusses the results for butane fuel supplied to the reactor at a concentration of 10,000 ppmC in nitrogen. Figures 4–7 show the measured concentration of detected gaseous species during butane pyrolysis at four sample probe inlet temperatures of 869 °C, 1018 °C, 1120 °C and 1213 °C, and a range of residence times.

Figure 4 shows that at the lowest temperature of 869 °C and all residence times sampled, ethylene was the most abundant stable species of butane pyrolysis; other abundant species detected in the gas sample withdrawn from the reactor at 869 °C were methane and acetylene. Ethane and propene were also detected in significant concentrations but only at the lowest residence times of 0.65 s and 0.98 s; as the residence time increased further to 1.31 s and 1.63 s and finally to 1.96 s, the concentrations of both species gradually decreased to very small levels. At just detectable concentrations, propyne, 1,3 butadiene, vinyl acetylene and benzene were also found.

As the concentration of ethylene was consistently an order of magnitude greater than that of ethane, this suggests that the formation of ethylene via ethane dehydrogenation was not a dominant pathway; more likely, ethylene was produced directly from dehydrogenation and C-C bond cleavage of butane as represented by the following reaction [52,53].

$$C_4H_{10} \rightarrow 2C_2H_4 + H_2$$

It can also be seen that the yield of methane remained relatively constant at this lowest temperature of 869 °C, regardless of residence time. This further reaffirms that methane was stable at this low temperature (discussed previously in Section 4.1, on methane pyrolysis) and suggests that methane is a terminal product not participating in further reactions during butane pyrolysis at 869 °C. It can be observed from Figure 4 that butane pyrolysis, in addition to C_1 and C_2 hydrocarbons, also produced small concentrations of C_3 and C_4 species. The presence of C_3 and C_4 species suggests the possibility of a greater number of reaction pathways for benzene formation and growth relative to those available during pyrolysis of methane and ethane at 869 °C, when C_3 and C_4 species were absent. For example, the C_3 hydrocarbons propene and propyne could convert into a propargyl radical, which, along with 1,3 butadiene and vinyl acetylene, are important precursors for formations of the first aromatic ring [54,55].

At the higher temperature of 1018 °C (Figure 5), similar trends to those observed at 869 °C can be seen (Figure 4), with the concentrations of ethylene, ethane, propyne and benzene decreasing with an increase in residence time, while the concentration of acetylene increased. The concentration of methane again remained constant at all residence times at this somewhat higher temperature of 1018 °C. It is also interesting to note that the relative proportions of various detected species were the same as those at the lower temperature of 869 °C, although the absolute concentrations were significantly smaller. It can be seen from Figure 5 that at 1018 °C, propyne and 1,3 butadiene were not detected at any of the residence times sampled. The relatively lower concentration of all species at 1018 °C (Figure 5) as compared to 869 °C (Figure 4) suggests increased reaction rates at the higher temperature, resulting in accelerated conversion to benzene, formed from smaller species, and simultaneously rapid conversion of benzene into PAHs [24,47].

At the next highest temperature of 1120 °C, Figure 6 shows that vinyl acetylene was no longer detected, while Figure 7 shows that at the highest temperature of 1213 °C, ethane and propene were also not found at any of the residence times sampled. The complete disappearance of ethane suggests that the equilibrium between C_2 species shifted to a greater level of dehydrogenation, and thus a greater relative abundance of the unsaturated species ethylene and acetylene. At the highest temperature of 1213 °C and the longest residence time of 1.51 s, methane, ethane and ethylene were all absent (Figure 7), indicating rapid dehydrogenation of these saturated and partially saturated species.

If the species concentrations at the lower temperatures of 869 °C and 1018 °C (Figures 4 and 5) are compared with concentrations at the higher temperatures of 1120 °C and 1213 °C (Figures 6 and 7), the major species found at the lower temperatures were ethylene, methane, ethane, acetylene and propene, with the addition of small concentrations of 1,3 butadiene, vinyl acetylene and benzene; in contrast, at the higher temperatures of 1120 °C and 1213 °C, the concentrations of detected species were drastically reduced. It is possible that this drastic reduction in species concentrations at the higher temperatures was the result of an accelerated conversion of benzene (itself formed rapidly from smaller species) into larger PAH molecules, as previously reported at these temperatures [24].

The presence of C_4 species at only very low concentrations at the lowest temperature of 869 °C, and the absence of significant concentrations of C_4 species at the higher temperatures, suggests that only a minor portion of butane fuel decomposed through H-loss pathways to form C_4 products [52], and that the relative importance of this route was unlikely to have been overly influenced by pyrolysis temperature.

It is interesting to note from Figures 4 and 5 that in the case of butane, the increase in temperature from 869 to 1018 °C caused a substantial reduction in concentrations of various species at all residence times, and that the effect of residence time is only secondary in the case of both temperatures.

In conclusion, during butane pyrolysis, ethylene was the most abundant species detected, which suggests that C-C bond cleavage was significant. It also suggests that along with acetylene, ethylene contributes to molecular mass growth. However, the presence of some C_3 and C_4 species implies that more reaction pathways were available for

benzene formation and further growth to PAHs. This suggestion is reinforced somewhat by visual observations made during the pyrolysis experiments of increased soot concentration emerging from the top of the reactor, and by results reported previously [24]. The more rapid depletion of C_3 species relative to C_2 also suggests the preferential formation of benzene via the propargyl pathways.

4.4. Effect of Carbon Chain Length on the Intermediate Species Formation

The discussion in Section 4.1, Section 4.2 and Section 4.3 shows that there are significant differences in the response of the fuels to increasing reactor temperature and pyrolysis residence time. The different responses in initial molecule decomposition, overall distribution of intermediate species, likely pathways for first ring formation, and equilibrium between different detected species at different temperatures and residence times are likely to be attributable to differences in molecular structure. A clear difference between the three fuel molecules was that methane, being the simplest alkane hydrocarbon, needed much higher initiation temperatures for its decomposition as compared to the two higher alkane fuels, ethane and butane. Further, during ethane and butane pyrolysis at lower temperatures, the concentration of methane produced remained constant, confirming its stable nature at lower temperatures.

It was previously reported in the literature that during methane pyrolysis, the initial decomposition of methane is by the breaking of the C-H bond via H abstraction, which produced methyl radicals [49]. Methyl radicals along with acetylene can play an important role in the formation of the first aromatic ring. Methyl radical concentration was not measured during the experiments, however, acetylene formed at higher temperatures (Figure 5) was readily detected. Once acetylene molecules form, they could combine with methyl radicals, resulting in the fast formation of propargyl radicals, followed by self-recombination of two propargyl radicals to form the first aromatic ring [56]. C_3 intermediate species were not detected during methane pyrolysis, suggesting the possibility that, if formed, they might have rapidly converted into benzene. In the case of ethane pyrolysis at the lower temperatures and smaller residence times, the concentration of methane detected was considerably lower than the concentration of ethylene, suggesting that the initial breakdown of the ethane molecules was mostly through dehydrogenation, rather than through C-C bond cleavage, to form ethylene (Figures 4 and 5). However, as the temperature rose, the concentration of acetylene relative to the concentration of ethylene increased considerably, suggesting further dehydrogenation of ethylene to form acetylene (Figures 6 and 7 compared with Figures 4 and 5). Therefore, it is suggested that at lower temperatures, ethylene is accumulated, while at higher temperatures, the higher concentration of acetylene plays a significant role in the formation of the first aromatic ring and PAH growth via the HACA mechanism. In the case of butane pyrolysis, a higher concentration of ethylene was observed at lower temperatures (Figure 4a), as compared to ethane and methane species, which suggests that the initial decomposition of butane was via C-C cleavage. The presence of C_3 and C_4 species along with C_1 and C_2 species during butane pyrolysis at lower temperatures suggests that in addition to those involving C_2 species, further reaction pathways were only available at lower temperatures for first ring formation. The detected C_3 species might readily have converted to propargyl radicals and 1,3 butadiene and vinyl acetylene, which are important precursors to benzene formation [57,58].

Dehydrogenation reactions appear to be most significant in the formation of acetylene during the pyrolysis of the small hydrocarbon fuels considered. The dehydrogenation processes are reversible, and temperature and pressure determine the equilibrium rates [59]. It has been reported that higher temperatures favour dehydrogenation reactions [32]. From Sections 4.1–4.3, it was observed that the equilibrium between the C_2 species (especially ethylene and acetylene) was shifted more toward acetylene formation at higher temperatures and longer residence times for all three fuels considered, especially in the case of methane relative to ethane and butane.

5. Conclusions

The effectiveness of a novel high-temperature air-cooled ceramic sampling probe and a new proposed methodology for quantifying fuel decomposition products were tested during the pyrolysis of methane, ethane and butane in a laminar flow reactor.

The results obtained showed good agreement with previous studies and the following specific conclusions drawn:

1. Methane pyrolysis required considerably higher temperature to initiate pyrolytic decomposition compared to lower temperatures required for ethane and butane decomposition. The major gaseous intermediate species detected during methane pyrolysis were C_2 (ethane, ethylene, and acetylene) and C_6 (benzene), implying that the first ring formation likely occurred via acetylene tricyclomerisation.
2. Temperature and residence time both influenced ethane breakdown routes. Ethane pyrolysis resulted in a higher concentration of C_2 intermediate species (ethylene and acetylene) relative to methane, suggesting that pyrolytic breakdown of ethane was mainly via dehydrogenation processes. Ethane and methane appear to undergo identical decomposition pathways, since both fuels primarily resulted in C_1, C_2, and C_6 (benzene) intermediate species.
3. During butane pyrolysis, the detection of C_1 and C_2 species suggested that, similarly to methane and ethane, the main pathways to form benzene were via C_2 species; in addition, the existence of certain C_3 and C_4 species implied further reaction pathways for benzene formation are likely to have been available, resulting in additional soot mass and PAHs.
4. In the case of butane, increasing the temperature from 869 to 1018 °C resulted in a significant decrease in concentrations of detected species at all residence times, and the influence of residence time was only secondary in the case of both temperatures.
5. Acetylene was a common species in the pyrolysis of all three alkane fuels, which would have served as a precursor to both PAHs formation via cyclisation as well as PAH surface growth via the HACA mechanism. Dehydrogenation processes appear to be the most important in the formation of acetylene. At higher temperatures and longer residence times, the equilibrium between the C_2 species (particularly ethylene and acetylene) moved towards acetylene formation for all three fuels studied.

Author Contributions: Conceptualization, Z.A.K., P.H. and N.L.; Methodology, Z.A.K., P.H. and N.L.; Software, Z.A.K., P.H. and A.A.; Validation, Z.A.K.; Formal analysis, Z.A.K.; Investigation, Z.A.K.; Resources, P.H.; Data curation, Z.A.K., P.H. and N.L.; Writing—original draft, Z.A.K.; Writing—review & editing, P.H., N.L. and A.A.; Visualization, Z.A.K. and A.A.; Supervision, P.H. and N.L.; Project administration, Z.A.K. and P.H.; Funding acquisition, P.H. All authors have read and agreed to the published version of the manuscript.

Funding: This research was funded by UK EPSRC grant number EP/M007960/1, And the APC was funded by University College London (UCL).

Institutional Review Board Statement: Not applicable.

Informed Consent Statement: Not applicable.

Data Availability Statement: Not applicable.

Acknowledgments: The first author is grateful to the Islamic Development Bank for sponsoring their research studies at University College London (UCL) and also acknowledges the support of the UK EPSRC (EP/M007960/1).

Conflicts of Interest: The authors declare no conflict of interest.

References

1. Masson-Delmotte, V.; Zhai, P.; Pirani, A.; Connors, S.L.; Péan, C.; Berger, S.; Caud, N.; Chen, Y.; Goldfarb, L.; Gomis, M.I.; et al. *Climate Change 2021: The Physical Science Basis*; Cambridge University Press: Cambridge, UK, 2021. [CrossRef]
2. Marris, C.R.; Kompella, S.N.; Miller, M.R.; Incardona, J.P.; Brette, F.; Hancox, J.C.; Sørhus, E.; Shiels, H.A. Polyaromatic hydrocarbons in pollution: A heart-breaking matter. *J. Physiol.* **2020**, *598*, 227–247. [CrossRef]

3. Inal, O.B.; Charpentier, J.F.; Deniz, C. Hybrid power and propulsion systems for ships: Current status and future challenges. *Renew. Sustain. Energy Rev.* **2022**, *156*, 111965. [CrossRef]
4. Verger, T.; Azimov, U.; Adeniyi, O. Biomass-based fuel blends as an alternative for the future heavy-duty transport: A review. *Renew. Sustain. Energy Rev.* **2022**, *161*, 112391. [CrossRef]
5. European Commission. Renewable Energy Directive. Eur Union 2021. Available online: https://energy.ec.europa.eu/topics/renewable-energy/renewable-energy-directive-targets-and-rules/renewable-energy-directive_en (accessed on 1 July 2021).
6. Keramiotis, C.; Vourliotakis, G.; Skevis, G.; Founti, M.A.; Esarte, C.; Sánchez, N.E.; Millera, A.; Bilbao, R.; Alzueta, M.U. Experimental and computational study of methane mixtures pyrolysis in a flow reactor under atmospheric pressure. *Energy* **2012**, *43*, 103–110. [CrossRef]
7. Xu, C.; Al Shoaibi, A.S.; Wang, C.; Carstensen, H.H.; Dean, A.M. Kinetic modeling of ethane pyrolysis at high conversion. *J. Phys. Chem. A* **2011**, *115*, 10470–10490. [CrossRef]
8. Marinov, N.M.; Pitz, W.J.; Westbrook, C.K.; Vincitore, A.M.; Castaldi, M.J.; Senkan, S.M.; Melius, C.F. Aromatic and polycyclic aromatic hydrocarbon formation in a laminar premixed n-butane flame. *Combust. Flame* **1998**, *114*, 192–213. [CrossRef]
9. Dong, L.L.; Cheung, C.S.; Leung, C.W. Heat transfer from an impinging premixed butane/air slot flame jet. *Int. J. Heat Mass Transf.* **2002**, *45*, 979–992. [CrossRef]
10. Kronemayer, H.; Barzan, D.; Horiuchi, M.; Suganuma, S.; Tokutake, Y.; Schulz, C.; Bessler, W.G. A direct-flame solid oxide fuel cell (DFFC) operated on methane, propane, and butane. *J. Power Sources* **2007**, *166*, 120–126. [CrossRef]
11. Hirasawa, T.; Sung, C.J.; Joshi, A.; Yang, Z.; Wang, H.; Law, C.K. Determination of laminar flame speeds using digital particle image velocimetry: Binary fuel blends of ethylene, n-butane, and toluene. *Proc. Combust. Inst.* **2002**, *29*, 1427–1434. [CrossRef]
12. Dong, Y.; Vagelopoulos, C.M.; Spedding, G.R.; Egolfopoulos, F.N. Measurement of laminar flame speeds through digital particle image velocimetry: Mixtures of methane and ethane with hydrogen, oxygen, nitrogen, and helium. *Proc. Combust. Inst.* **2002**, *29*, 1419–1426. [CrossRef]
13. Göttgens, J.; Mauss, F.; Peters, N. Analytic Approximations of Burning Velocities and Flame Thicknesses of Lean Hydrogen, Methane, Ethylene, Ethane, Acetylene, and Propane Flames. In *Symposium (International) on Combustion*; Elsevier: Amsterdam, The Netherlands, 1992; Volume 24, pp. 129–135. [CrossRef]
14. Turányi, T.; Zádor, J.; Zsély, I.G. Local and global uncertainty analyses of a methane flame model. *J. Phys. Chem.* **2005**, *228*, 9795–9807. [CrossRef]
15. Bradley, D.; Gaskell, P.H.; Gu, X.J. Burning velocities, Markstein lengths, and flame quenching for spherical methane-air flames: A computational study. *Combust. Flame* **1996**, *104*, 176–198. [CrossRef]
16. Egolfopoulos, F.N.; Cho, P.; Law, C.K. Laminar flame speeds of methane-air mixtures under reduced and elevated pressures. *Combust. Flame* **1989**, *76*, 375–391. [CrossRef]
17. Li, W.; Wang, G.; Li, Y.; Li, T.; Zhang, Y.; Cao, C.; Zou, J.; Law, C.K. Experimental and kinetic modeling investigation on pyrolysis and combustion of n-butane and i-butane at various pressures. *Combust. Flame* **2018**, *191*, 126–141. [CrossRef]
18. Stadnichenko, O.A.; Snytnikov, V.N.; Snytnikov, V.N.; Masyuk, N.S. Mathematical modeling of ethane pyrolysis in a flow reactor with allowance for laser radiation effects. *Chem. Eng. Res. Des.* **2016**, *109*, 405–413. [CrossRef]
19. Hashemi, H.; Jacobsen, J.G.; Rasmussen, C.T.; Christensen, J.M.; Glarborg, P.; Gersen, S.; van Essen, M.; Levinsky, H.B.; Klippenstein, S.J. High-pressure oxidation of ethane. *Combust. Flame* **2017**, *182*, 150–166. [CrossRef]
20. Naik, C.V.; Dean, A.M. Detailed kinetic modeling of ethane oxidation. *Combust. Flame* **2006**, *145*, 16–37. [CrossRef]
21. Kikui, S.; Kamada, T.; Nakamura, H.; Tezuka, T.; Hasegawa, S.; Maruta, K. Characteristics of n-butane weak flames at elevated pressures in a micro flow reactor with a controlled temperature profile. *Proc. Combust. Inst.* **2015**, *35*, 3405–3412. [CrossRef]
22. Klotz, S.D.; Brezinsky, K.; Glassman, I. Modeling the Combustion of Toluene-Butane Blends. In *Symposium (International) on Combustion*; Elsevier: Amsterdam, The Netherlands, 1998; Volume 27, pp. 337–344. [CrossRef]
23. Dandajeh, H.A.; Ladommatos, N.; Hellier, P.; Eveleigh, A. Effects of unsaturation of C2 and C3 hydrocarbons on the formation of PAHs and on the toxicity of soot particles. *Fuel* **2017**, *194*, 306–320. [CrossRef]
24. Dandajeh, H.A.; Ladommatos, N.; Hellier, P.; Eveleigh, A. In fluence of carbon number of C1–C7 hydrocarbons on PAH formation. *Fuel* **2018**, *228*, 140–151. [CrossRef]
25. Kaiser, E.W.; Siegl, W.O.; Cotton, D.F.; Anderson, R.W. Effect of Fuel Structure on Emissions from a Spark-Ignited Engine. 3. Olefinic Fuels. *Environ. Sci. Technol.* **1993**, *27*, 1440–1447. [CrossRef]
26. Karim, G.A. Combustion in gas fueled compression: Ignition engines of the dual fuel type. *J. Eng. Gas Turbines Power* **2003**, *125*, 827–836. [CrossRef]
27. Selim, M.Y.E. Sensitivity of dual fuel engine combustion and knocking limits to gaseous fuel composition. *Energy Convers. Manag.* **2004**, *45*, 411–425. [CrossRef]
28. Gerö, L. Bond Energies of Hydrocarbons. *J. Chem. Phys.* **2004**, *16*, 1011. [CrossRef]
29. Bernstein, H.J. Bond energies in hydrocarbons. *Trans. Faraday Soc.* **1962**, *58*, 2285–2306. [CrossRef]
30. Glassman, I.; Yetter, R.A.; Glassman, I. *Combustion*, 4th ed.; Academic Press: Cambridge, MA, USA, 2008.
31. Guéret, C.; Daroux, M.; Billaud, F. Methane pyrolysis: Thermodynamics. *Chem. Eng. Sci.* **1997**, *52*, 815–827. [CrossRef]
32. Murphy, D.B.; Carroll, R.W.; Klonowski, J.E. Analysis of products of high-temperature pyrolysis of various hydrocarbons. *Carbon* **1997**, *35*, 1819–1823. [CrossRef]

33. Bunker, C.E.; Deblase, A.F.; Youtsler, T.A.; Sanders, N.L.; Lewis, W.K. Enhanced Bimolecular Reaction in a Two-Component Fluid under Pyrolytic Conditions: In Situ Probing of the Pyrolysis of Jet Fuel Surrogates Using a Supersonic Expansion Molecular Beam Mass Spectrometer. *Energy Fuels* **2018**, *32*, 3391–3398. [CrossRef]
34. Dryer, F.L.; Glassman, I. High-temperature oxidation of CO and CH_4. In *Symposium (International) on Combustion*; Elsevier: Amsterdam, The Netherlands, 1973; Volume 14, pp. 987–1003. [CrossRef]
35. Frost, J.; Hellier, P.; Ladommatos, N. A systematic study into the effect of lignocellulose-derived biofuels on the combustion and emissions of fossil diesel blends in a compression ignition engine. *Fuel* **2022**, *313*, 122663. [CrossRef]
36. Russo, C.; Alfe, M.; Rouzaud, J.N.; Stanzione, F.; Tregrossi, A.; Ciajolo, A. Probing structures of soot formed in premixed flames of methane, ethylene and benzene. *Proc. Combust. Inst.* **2013**, *34*, 1885–1892. [CrossRef]
37. Boehm, H.; Jander, H.; Tanke, D. PAH Growth and Soot Formation in the Pyrolysis of Acetylene and Benzene at High Temperatures and Pressures: Modeling and Experiment. In *Symposium (International) on Combustion*; Elsevier: Amsterdam, The Netherlands, 1998; Volume 1, pp. 1605–1612.
38. McEnally, C.S.; Pfefferle, L.D. The effects of dimethyl ether and ethanol on benzene and soot formation in ethylene nonpremixed flames. *Proc. Combust. Inst.* **2007**, *31*, 603–610. [CrossRef]
39. Richter, H.; Grieco, W.J.; Howard, J.B. Formation mechanism of polycyclic aromatic hydrocarbons and fullerenes in premixed benzene flames. *Combust. Flame* **1999**, *119*, 1–22. [CrossRef]
40. Bruinsma, O.S.L.; Moulijn, J.A. The pyrolytic formation of polycyclic aromatic hydrocarbons from benzene, toluene, ethylbenze,e, styrene, phenylacetylene and n-decane in relation to fossil fuels utilization. *Fuel Process. Technol.* **1988**, *18*, 213–236. [CrossRef]
41. Liu, P.; Li, Z.; Bennett, A.; Lin, H.; Sarathy, S.M.; Roberts, W.L. The site effect on PAHs formation in HACA-based mass growth process. *Combust. Flame* **2019**, *199*, 54–68. [CrossRef]
42. Wang, H.; Frenklach, M. A detailed kinetic modeling study of aromatics formation in laminar premixed acetylene and ethylene flames. *Combust. Flame* **1997**, *110*, 173–221. [CrossRef]
43. Eveleigh, A.; Ladommatos, N.; Hellier, P.; Jourdan, A.L. Quantification of the Fraction of Particulate Matter Derived from a Range of 13C-Labeled Fuels Blended into Heptane, Studied in a Diesel Engine and Tube Reactor. *Energy Fuels* **2016**, *30*, 7678–7690. [CrossRef]
44. Marsh, N.D.; Ledesma, E.B.; Sandrowitz, A.K.; Wornat, M.J. Yields of Polycyclic Aromatic Hydrocarbons from the Pyrolysis of Catechol [ortho-Dihydroxybenzene]: Temperature and Residence Time Effects. *Energy Fuels* **2004**, *18*, 209–217. [CrossRef]
45. Eveleigh, A.; Ladommatos, N.; Balachandran, R.; Marca, A. Conversion of oxygenated and hydrocarbon molecules to particulate matter using stable isotopes as tracers. *Combust. Flame* **2014**, *161*, 2966–2974. [CrossRef]
46. Eveleigh, A.; Ladommatos, N.; Hellier, P.; Jourdan, A. An investigation into the conversion of specific carbon atoms in oleic acid and methyl oleate to particulate matter in a diesel engine and tube reactor. *Fuel* **2015**, *153*, 604–611. [CrossRef]
47. Khan, Z.A.; Hellier, P.; Ladommatos, N. Measurement of soot mass and PAHs during the pyrolysis of C_2—C_4 alcohols at high temperatures. *Combust. Flame* **2022**, *236*, 111803. [CrossRef]
48. Matar, S.; Hatch, L.F. (Eds.) Chapter Two—Hydrocarbon Intermediates. In *Chemistry of Petrochemical Processes*, 2nd ed.; Gulf Professional Publishing: Woburn, UK, 2001; pp. 29–48. [CrossRef]
49. Khan, M.S.; Crynes, B.L. Survey of Recent Methane Pyrolysis Literature. *Ind. Eng. Chem.* **1970**, *62*, 54–59. [CrossRef]
50. Richter, H.; Howard, J.B. Formation of polycyclic aromatic hydrocarbons and their growth to soot-a review of chemical reaction pathways. *Prog. Energy Combust. Sci.* **2000**, *26*, 565–608. [CrossRef]
51. Nurislamova, L.F.; Stoyanovskaya, O.P.; Stadnichenko, O.A.; Gubaidullin, I.M.; Snytnikov, V.N.; Novichkova, A.V. Few-step kinetic model of gaseous autocatalytic ethane Pyrolysis and its evaluation by means of uncertainty and sensitivity analysis. *Chem. Prod. Process Model.* **2014**, *9*, 143–154. [CrossRef]
52. Zhang, Y.J.; Yuan, W.H.; Cai, J.H.; Zhang, L.D.; Qi, F.; Li, Y.Y. Product identification and mass spectrometric analysis of n-butane and i-butane pyrolysis at low pressure. *Chin. J. Chem. Phys.* **2013**, *26*, 151–156. [CrossRef]
53. Sandler, S.; Chung, Y. High-Temperature Pyrolysis of n-Butane. *Ind. Eng. Chem.* **1961**, *53*, 391–394. [CrossRef]
54. Cole, J.A.; Bittner, J.D.; Longwell, J.P.; Howard, J.B. Formation Mechanisms of Aromatic Compounds in Aiiphatic Flames. *Combust. Flame* **1984**, *56*, 51–70. [CrossRef]
55. Miller, J.A.; Melius, C.F. Kinetic and Thermodynamic Issues in the Formation of Aromatic Compounds in Flames of Aliphatic Fuels. *Combust. Flame* **1992**, *91*, 21–39. [CrossRef]
56. Eremin, A.; Mikheyeva, E. The Role of Methyl Radical in Soot Formation. *Combust. Sci. Technol.* **2019**, *191*, 2226–2242. [CrossRef]
57. Colket, M.B.; Seery, D.J. Reaction Mechanisms for Toluene Pyrolysis. In *Symposium (International) on Combustion*; Elsevier: Amsterdam, The Netherland, 1994; Volume 25, pp. 883–891. [CrossRef]
58. Appel, J.; Bockhorn, H.; Frenklach, M. Kinetic modeling of soot formation with detailed chemistry and physics: Laminar premixed flames of C_2 hydrocarbons. *Combust. Flame* **2000**, *121*, 122–136. [CrossRef]
59. Fahim, M.A.; Alsahhaf, T.A.; Elkilani, A. Chapter 5—Catalytic Reforming and Isomerization. In *Fundamentals of Petroleum Refining*; Elsevier: Amsterdam, The Netherland, 2010. [CrossRef]